

Article

Seasonal and Depth Dynamics of Soil Moisture Affect Trees on the Tibetan Plateau

Qian Li ^{1,2}, Liang Jiao ^{1,2,*} , Ruhong Xue ^{1,2}, Xichen Che ^{1,2}, Peng Zhang ^{1,2}, Xuge Wang ^{1,2} and Xin Yuan ^{1,2}

¹ College of Geography and Environmental Science, Northwest Normal University, No. 967, Anning East Road, Lanzhou 730070, China; liqian12080504@163.com (Q.L.); xrhnwnu@163.com (R.X.); chexichen1013@163.com (X.C.); zp1804059098@163.com (P.Z.); wangxuge2022@163.com (X.W.); yuanxin0503@163.com (X.Y.)

² Key Laboratory of Resource Environment and Sustainable Development of Oasis, Gansu Province, Northwest Normal University, Lanzhou 730070, China

* Correspondence: jiaoliang@nwnu.edu.cn; Tel.: +86-7971952

Abstract: The soil moisture (SM) influences tree growth with climate change. However, the spatial and temporal dynamics of tree water use strategies in climate-sensitive areas remain uncertain. Therefore, we collected the tree-ring oxygen isotope ($\delta^{18}\text{O}_{\text{TR}}$) chronologies and divided the wet–dry gradients according to the precipitation on the Tibetan Plateau (TP). Further, the relationship between the $\delta^{18}\text{O}_{\text{TR}}$ and environmental factors was analyzed across different gradients. We found the following: (1) The SM during the growing season was the most important factor for $\delta^{18}\text{O}_{\text{TR}}$. (2) The response of the $\delta^{18}\text{O}_{\text{TR}}$ to the SM had a lag in arid areas than in humid areas. (3) Trees absorbed the SM on the surface in humid areas ($r = -0.49$ to -0.41 , $p < 0.01$), while trees absorbed the SM from deep in the soil in arid areas ($r = -0.48$ to -0.29 , $p < 0.01$). The results demonstrated that trees were better able to cope with drought stress in arid regions because they used more stable deep soil water than in humid regions. Therefore, the findings will provide a scientific basis for water use of trees using the $\delta^{18}\text{O}_{\text{TR}}$ in complex environmental contexts. Trees with single water use strategies should be given more attention to keep ecosystems healthy.

Keywords: Tibetan Plateau (TP); tree-ring oxygen isotope ($\delta^{18}\text{O}_{\text{TR}}$); water use strategies; soil moisture; wet–dry gradients



Citation: Li, Q.; Jiao, L.; Xue, R.; Che, X.; Zhang, P.; Wang, X.; Yuan, X. Seasonal and Depth Dynamics of Soil Moisture Affect Trees on the Tibetan Plateau. *Forests* **2024**, *15*, 752. <https://doi.org/10.3390/f15050752>

Academic Editor: Matthew Therrell

Received: 24 March 2024

Revised: 21 April 2024

Accepted: 23 April 2024

Published: 25 April 2024



Copyright: © 2024 by the authors. Licensee MDPI, Basel, Switzerland. This article is an open access article distributed under the terms and conditions of the Creative Commons Attribution (CC BY) license (<https://creativecommons.org/licenses/by/4.0/>).

1. Introduction

Climate change has profound impacts on forest ecosystems [1,2]. Tree growth is mainly influenced by temperature, precipitation, and their interactions [3,4]. It is well known that tree growth in arid regions is controlled by soil moisture (SM), while in humid regions, it is mainly influenced by temperature [5]. Therefore, there is variability in the environmental sensitivity of trees in different climatic contexts.

The SM is the main source to sustain plant growth [6]. It plays a vital role in maintaining ecosystem health. The SM varies with soil seasons and depths [7]. There are also differences in the uptake strategies of SM by trees in different moisture environments [8]. Some studies have found that the SM plays a role in tree growth on the Tibetan Plateau (TP) [9,10], especially during the growing season [11]. Unfortunately, it is not practical to collect soil samples when conducting large-scale studies, making it exceptionally difficult to use measured soil data to study tree water use strategies. However, tree-ring oxygen isotope ($\delta^{18}\text{O}_{\text{TR}}$) is now used as an indicator to study long-term changes in the SM because of their stability [12]. For example, the SM for nearly a century has been reconstructed using the $\delta^{18}\text{O}_{\text{TR}}$ in the Western Himalayas [13].

The $\delta^{18}\text{O}_{\text{TR}}$ is jointly controlled by the coupled processes of transpiration and water uptake in tree root systems [14]. Therefore, the $\delta^{18}\text{O}_{\text{TR}}$ is an important indicator that can record the response of trees to seasonal climate change [15]. A complex set of $\delta^{18}\text{O}_{\text{TR}}$

formation processes are influenced by external climatic factors [16,17]. Trees absorb precipitation entering the soil and then preserve the precipitation signal in the $\delta^{18}\text{O}_{\text{TR}}$ through transpiration fractionation in the leaves [18,19].

The precipitation in monsoon areas has significant seasonal variations, and similar variations occur in the SM [20,21]. Thus, the $\delta^{18}\text{O}$ of SM varies at different depths and seasons. The $\delta^{18}\text{O}_{\text{TR}}$ stores SM signals through complex physiological mechanisms [22]. For example, it has been found that the $\delta^{18}\text{O}$ of *Pinus tabulaeformis* in the East Asian monsoon (EAM) zone is controlled by the SM [23]. And it has been shown that trees used the shallow SM in the wet season and deep water in the dry season in the EAM region [24].

The TP has been found to have a trend of increasing temperatures [25] and decreasing precipitation in recent years due to shifts in the Asian summer monsoons (ASMs) [26,27]. The $\delta^{18}\text{O}_{\text{TR}}$ was consequently affected in this region [28,29]. At present, there are many articles on the use of $\delta^{18}\text{O}_{\text{TR}}$ to study climate reconstruction and the interpretation of physiological mechanism on the TP [30–32]. There are few studies that have been conducted to use the $\delta^{18}\text{O}_{\text{TR}}$ to study water use strategies. Therefore, the purpose of this paper is to explore three main questions on the TP: (1) What are the seasonal dynamics of different gradients of SM use? (2) Is there a difference in the depth of water used by trees at different gradients? (3) Are the seasons as well as soil depths of different gradients of trees water use coupled?

2. Materials and Methods

2.1. Study Areas

As shown in Figure 1, we selected a total of six sampling points. The Delingha region (DE) is in the northeastern part of the TP. The Ganesh (GA) and Wache (WA) regions are in the southern of the TP. The Manali (MA) and Jageshwar (JA) regions are in the southwestern part of the TP. And the Karakorun region (KA) is in the west of the TP. The JA is the wettest region, and the DE is the driest region in our study (Figure 2). The difference in the annual total precipitation between these two regions is 1311 mm. On the basis of the annual total precipitation, the six regions are classified into humid areas (JA, WA, and GA regions) and arid areas (MA, KA, and DE regions).

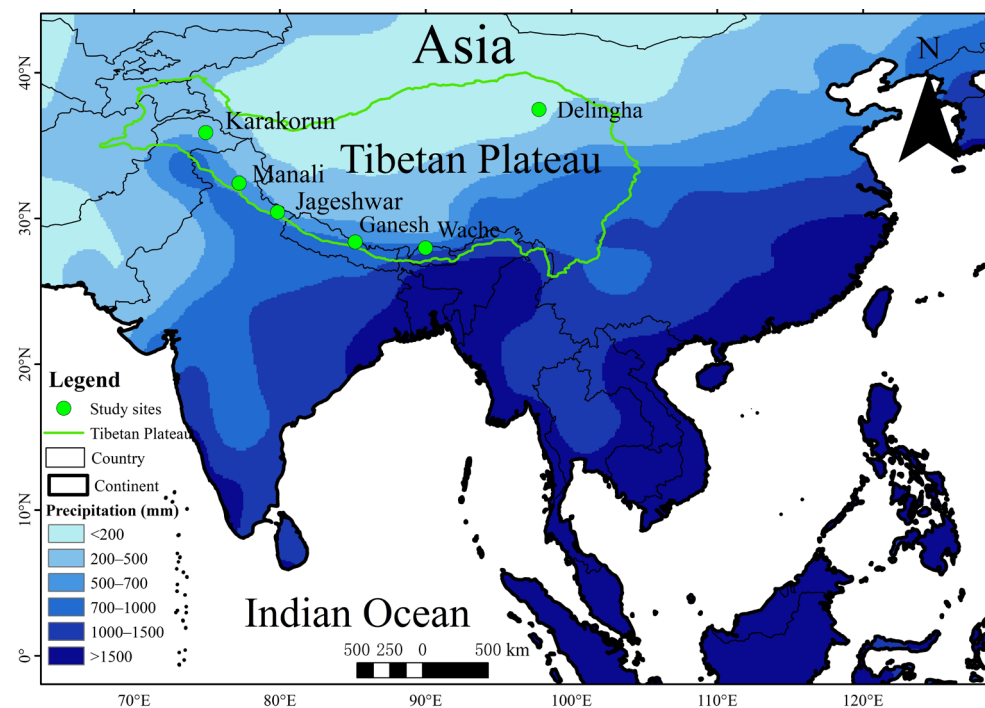


Figure 1. Geographical locations of study area and sampling sites.

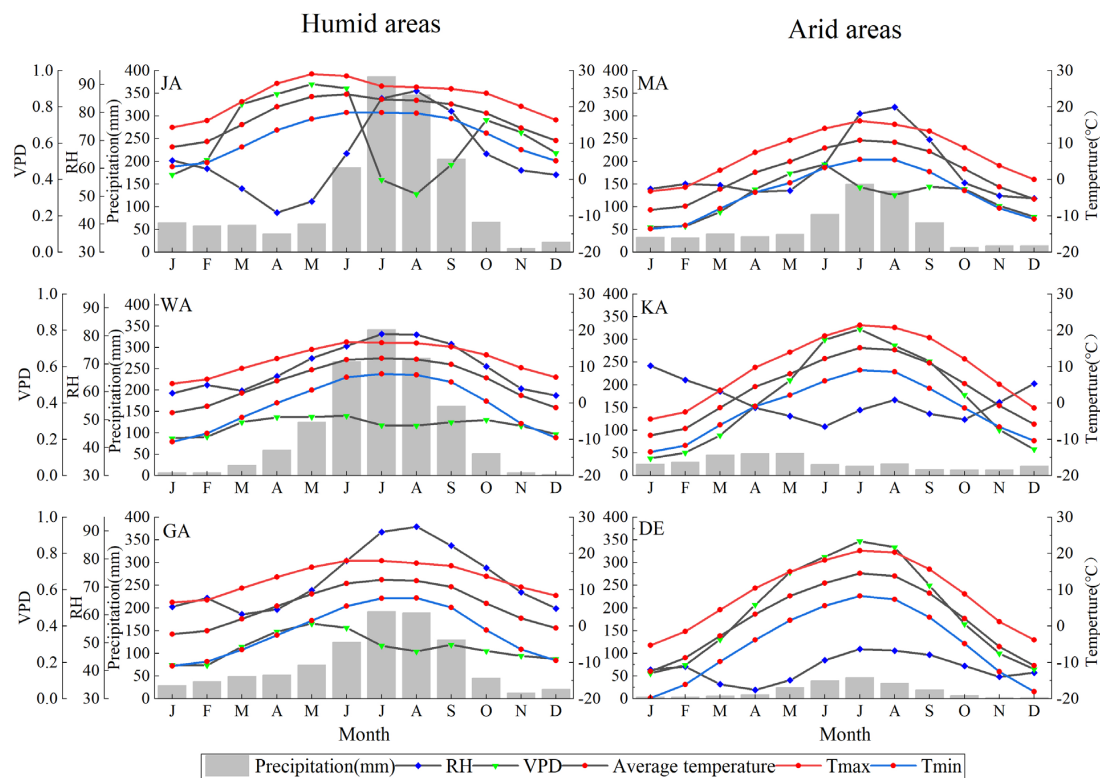


Figure 2. Meteorological elements of the study areas.

2.2. Tree-Ring Isotope Data

The $\delta^{18}\text{O}_{\text{TR}}$ data were downloaded from the NOAA Paleoclimatology Datasets (<https://www.ncsl.noaa.gov>, accessed on 26 August 2023). Table 1 provides specific information on the six sampling sites. The experimental methods were checked when downloading data to ensure that the same experimental methods did not affect the accuracy of the study [33]. Some scholars have already found that elevation and age do not affect the $\delta^{18}\text{O}_{\text{TR}}$ [34,35].

Table 1. The $\delta^{18}\text{O}_{\text{TR}}$ chronology information.

Sites	Location	Elevation (m)	Tree Species	Time Span	Annual Total Precipitation (mm)	Date Source
JA	29°38' N, 79°51' E	1870	<i>Cedrus deodara</i>	1621–2008	1505	Xu et al. (2018) [31]
WA	27°59' N, 90° E	3500	<i>Larix griffithii</i>	1743–2011	1330	Sano et al. (2013) [36]
GA	28°10' N, 85°11' E	3500	<i>Abies spectabilis</i>	1801–2000	958	Xu et al. (2018) [31]
MA	32°13' N, 77°13' E	2700	<i>Abies pindrow</i>	1768–2008	650	Sano et al. (2017) [32]
KA	35°54' N, 74°56' E	2900	<i>Juniperus excelsa</i>	1900–1998	329	Treydte et al. (2006) [37]
DE	37°48' N, 97°78' E	3500	<i>Juniperus przewalskii</i>	1168–2011	197	Yang et al. (2021) [38]

2.3. Meteorological Data

The maximum (Tmax), mean(T), and minimum temperatures (Tmin), precipitation (PRCP), and the Palmer drought severity index (PDSI) from Climate Explorer (<http://climexp.knmi.nl/start.cgi>, accessed on 28 August 2023) were calculated (Figure 2). These were monthly scale data for the subsequent study. The vapor pressure deficit (VPD) was calculated as in Equation (1) [39]. And relative humidity (RH) was calculated as in Equations (2) and (3) [40].

$$\begin{aligned} \text{VPD} &= \text{actual water vapour pressure} = \text{saturated water vapour pressure} \\ &= e^0 \times 10^{\left(\frac{7.5T}{T+237.3}\right)} - \text{actual water vapor pressure} \end{aligned} \quad (1)$$

$$\text{RH} = \left(\frac{e}{e_{\text{sat}}}\right) \times 100 \quad (2)$$

$$e_{\text{sat}} = 6.108 \times \exp(17.27 \times T / (T + 273.3)) \quad (3)$$

where $e^0 = 6.11$ hpa.

2.4. The SM Data

The SM data was obtained from the Global Land Data Assimilation System (<http://Idas.gsfc.nasa.gov/gldas>, accessed on 29 August 2023). It spans the period of 1948–2015, with a spatial resolution of $0.25^\circ \times 0.25^\circ$. Due to its good temporal and spatial resolutions, it has been used for a large number of studies in recent years. The SM data of three depths of 0–100 cm were selected. We transform the SM data (unit: kg/m^2) into volumetric water content (VWC, unit: m^3/m^3) according to Equation (4).

$$\text{VWC} = \frac{\text{kg}}{\text{m}^2} \times \frac{\text{m}^3}{1000\text{kg}} \times \frac{1000\text{mm}}{1\text{m}} \times \frac{1}{\text{thickness of layer in mm}} \quad (4)$$

2.5. Data Analysis

Pearson's correlation analysis as well as partial correlation analysis were used to study the main climatic factors affecting $\delta^{18}\text{O}_{\text{TR}}$. The variability in the $\delta^{18}\text{O}_{\text{TR}}$ chronology was tested using one-way analysis of variance (ANOVA) in different regions. Meanwhile, the spatial correlation analysis of the $\delta^{18}\text{O}_{\text{TR}}$ and the SM was performed using MATLAB 2023.

3. Results

3.1. The Spatial and Temporal Patterns of the $\delta^{18}\text{O}_{\text{TR}}$

Figure 3 shows that the values of the $\delta^{18}\text{O}_{\text{TR}}$ in the arid areas as a whole (31.36‰) were larger than those in the humid areas (24.34‰) on the TP. But the dynamics of $\delta^{18}\text{O}_{\text{TR}}$ showed inconsistent spatial and temporal variation characteristics across wet and dry gradients. In addition, the values of $\delta^{18}\text{O}_{\text{TR}}$ showed an increasing trend in all regions except the DE region. And the increasing trend was overall more pronounced in the humid areas.

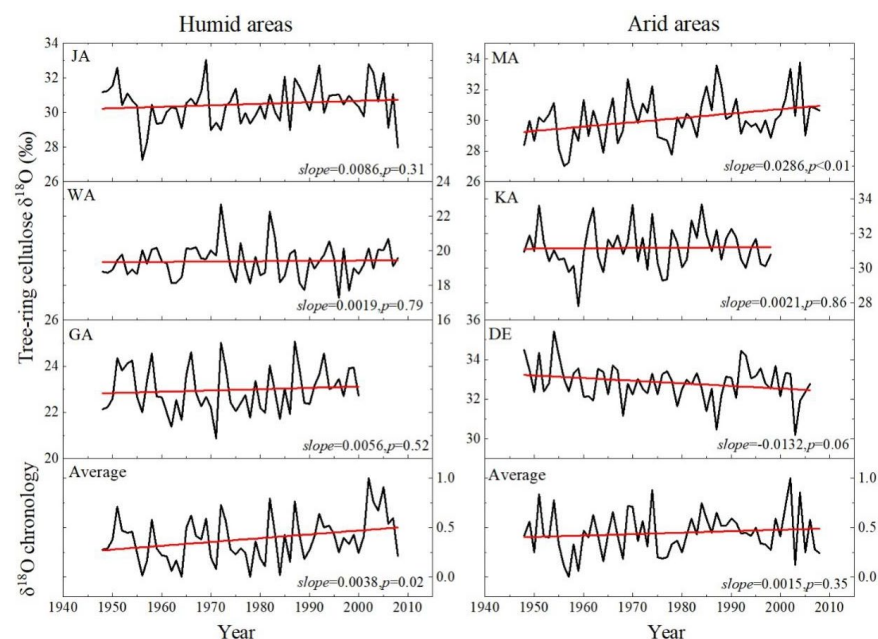


Figure 3. The time series of the $\delta^{18}\text{O}_{\text{TR}}$ for each site.

The spatial dynamics of the $\delta^{18}\text{O}_{\text{TR}}$ showed that, as the climate becomes wetter, the values of the $\delta^{18}\text{O}_{\text{TR}}$ declined (Figure 4). The $\delta^{18}\text{O}_{\text{TR}}$ values are the highest (DE, 32.90‰) on the northern of the TP. On the contrary, the $\delta^{18}\text{O}_{\text{TR}}$ values are the lowest (WA, 19.40‰) on the southern of the TP.

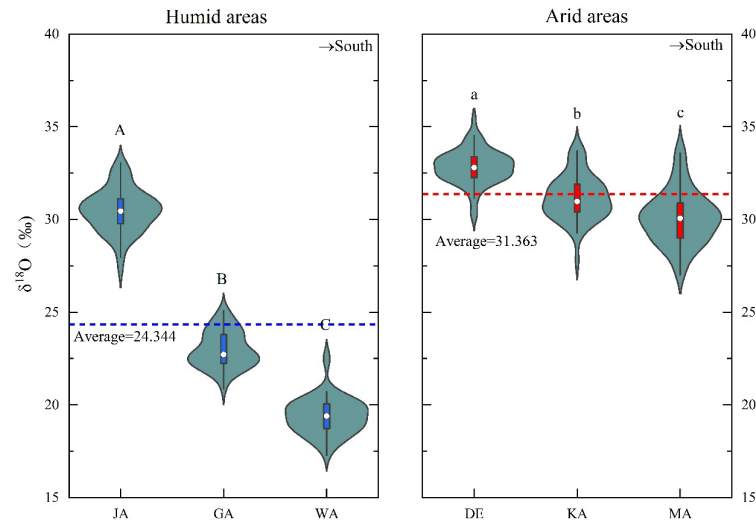


Figure 4. Significance test for study areas. Inter-sample differences in $\delta^{18}\text{O}_{\text{TR}}$ values were assessed using one-way ANOVA, with different letters indicating significant differences ($p < 0.05$).

3.2. The SM Dynamics at Different Depth Gradients

Figure 5 shows that the SM at different depths exhibits inconsistent variability characteristics on the TP (Figure 5). Specifically, the SM increased with a deeper soil depth (Figure 5a). And the SM in the DE region is much lower than in other regions.

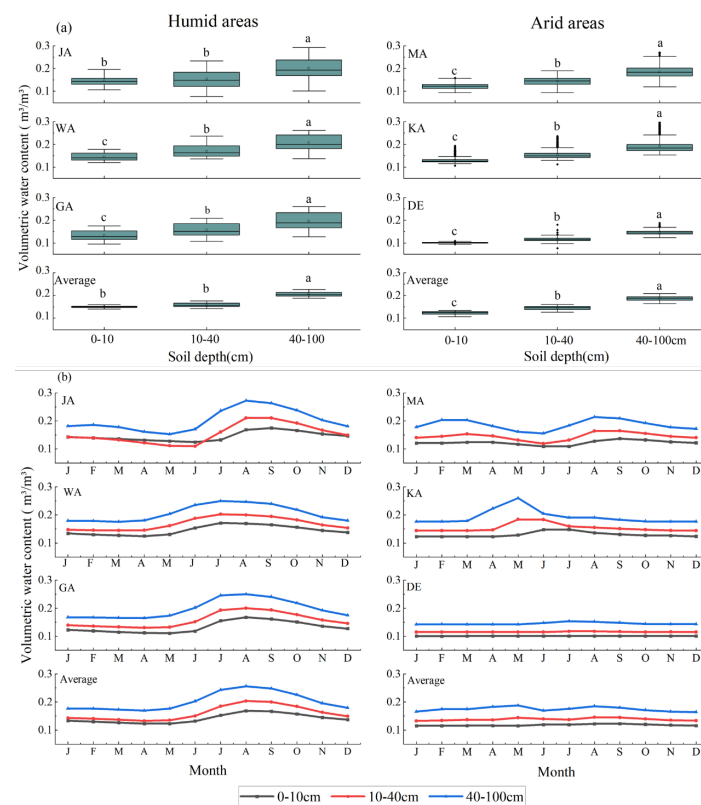


Figure 5. Dynamics of SM in different soil layers in different months. The squares in the boxplot diagram represent the median SM, different letters indicating significant differences ($p < 0.05$), the black

dots represent the outliers and the range of the boxes represents the 25%–75% data interval (a). The blue line in the graph represents the 40–100 cm volumetric water content, the red line represents the 10–40 cm volumetric water content and the black line represents the 0–10 cm volumetric water content (b).

Figure 5b shows that the seasonal dynamics of SM are more pronounced in humid areas. The high values of SM occur from June to September in humid areas ($VMC_{Jun-Sep} > 45\%$). However, this phenomenon does not occur in arid areas. In the MA region, the high values of SM occur from June to September ($VMC_{Jun-Sep} > 35\%$). The high values of VMC occur from April to June ($VMC_{Apr-Jun} > 32\%$) in the KA region. But no seasonal dynamic was observed in the SM in the driest DE region.

The wettest JA region showed a decreasing trend for the SM, while the driest DE region showed an increasing trend for the SM (Figure 6). Overall, the surface SM increased in the wetter areas, while middle and deeper SM decreased. In arid areas, the SM decreased by 40–100 cm and increased by 0–40 cm. Meanwhile, it was found that the SM in humid areas fitted better with precipitation (Figure 7).

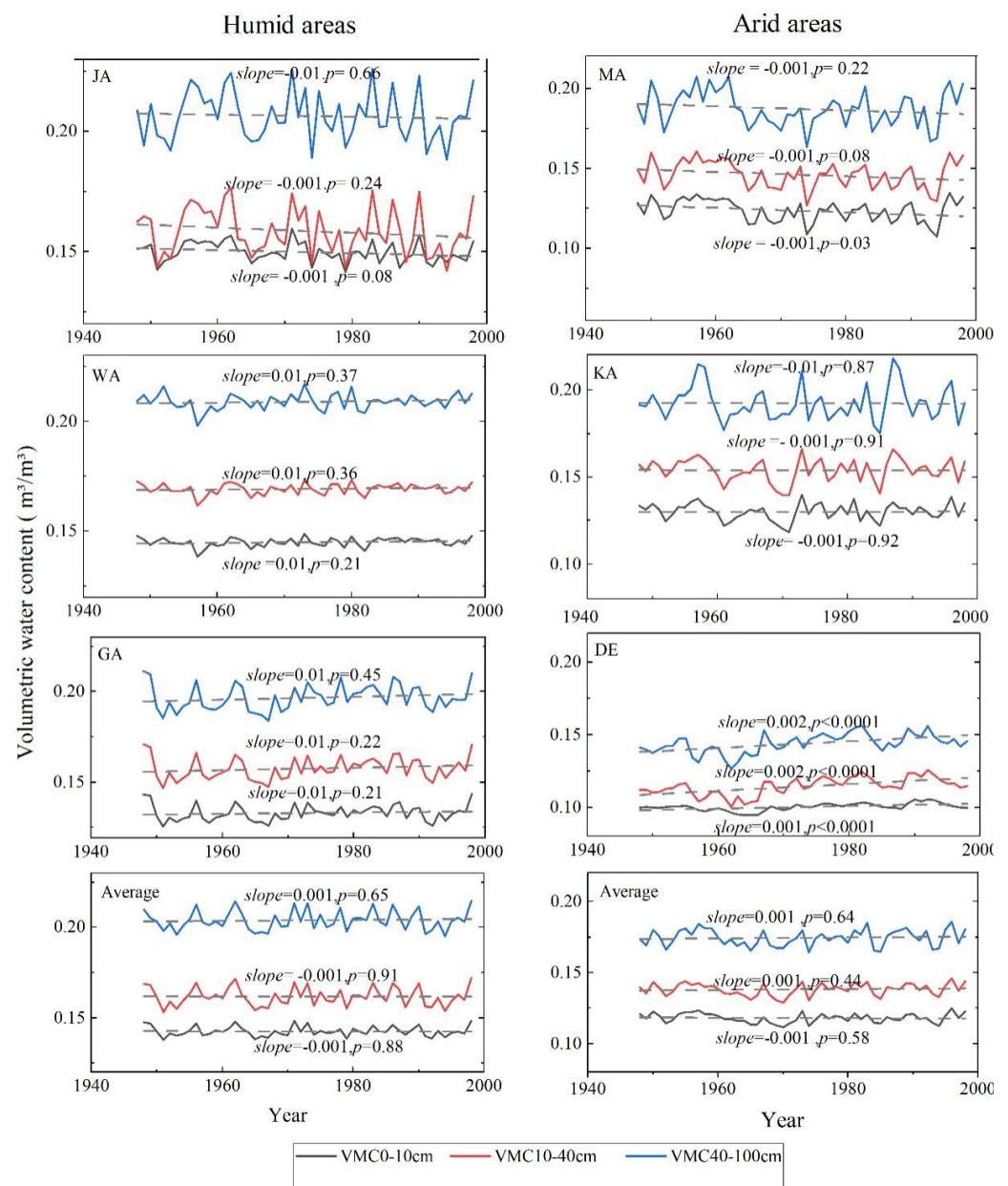


Figure 6. Interannual variation in SM.

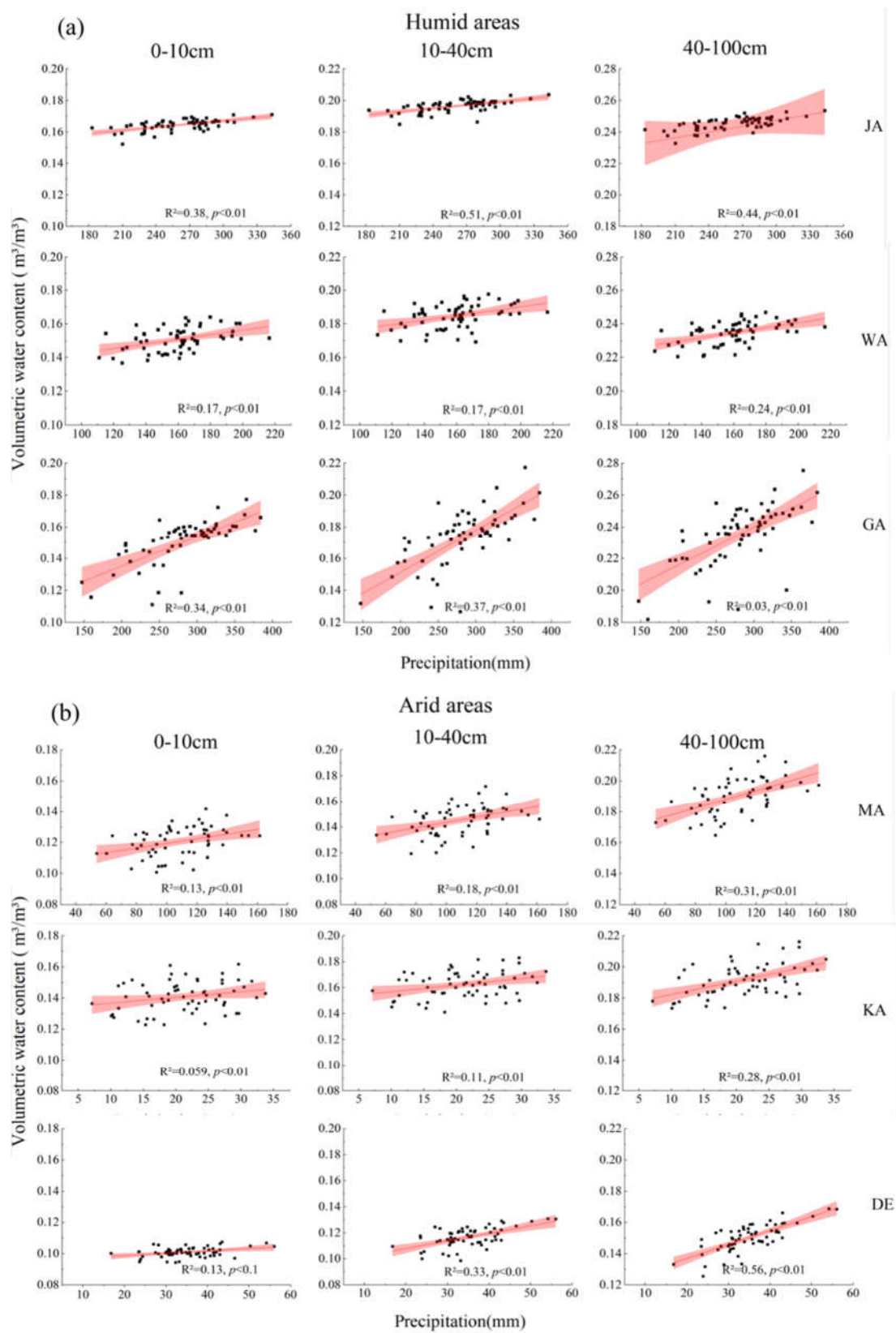


Figure 7. Linear fitting of SM and precipitation. The red area in the graph represents the 95% confidence interval and the red line represents the fitted trend line.

3.3. The Response of $\delta^{18}O_{TR}$ to Climatic and SM Factors

It is revealed that the overall $\delta^{18}O_{TR}$ responded negatively to PDSI, PRCP, and RH (Figure 8). The $\delta^{18}O_{TR}$ is positively correlated with T, Tmax, Tmin, and VPD in study areas (Figure 8). And $\delta^{18}O_{TR}$ in the humid areas are mainly influenced by climatic factors during the middle of the growing season in the humid areas and during the late growing season in the arid areas.

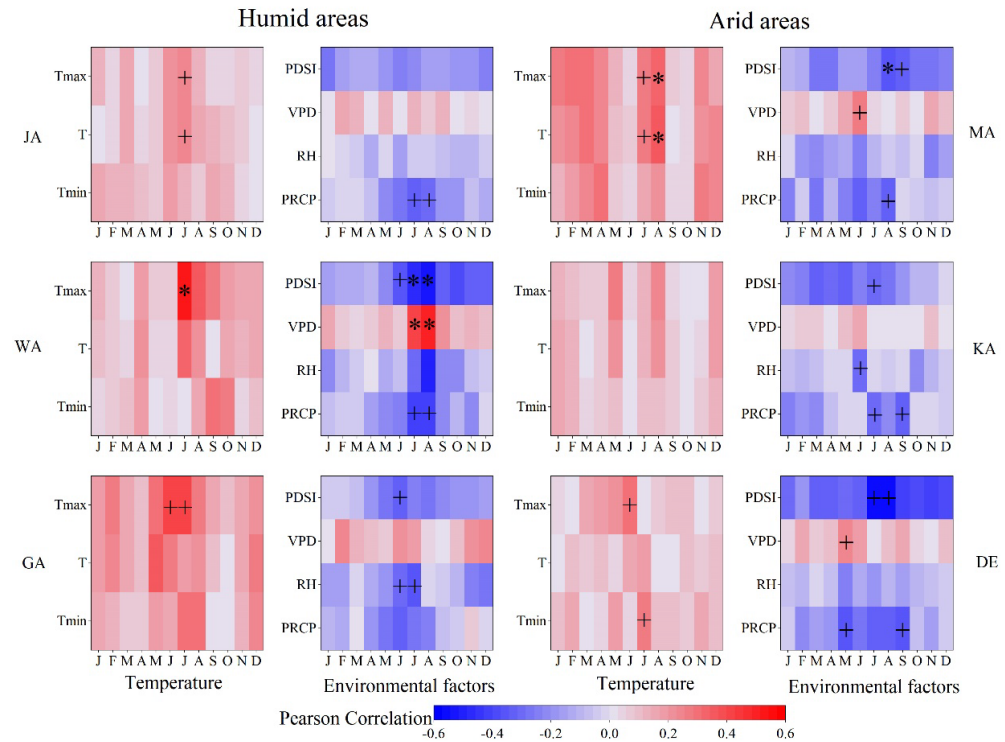


Figure 8. Correlations of $\delta^{18}O_{TR}$ with monthly climate variables. “+”: significant correlations at 95%. “**”: significant correlations at 99%.

The response of the $\delta^{18}O_{TR}$ to the SM in terms of season and depth were further investigated (Figure 9). The correlation between the $\delta^{18}O_{TR}$ and the SM was greater with $SM_{0-10\text{ cm}}$ and $SM_{10-40\text{ cm}}$ in July in humid areas. However, the $\delta^{18}O_{TR}$ was significantly negatively correlated with $SM_{10-40\text{ cm}}$ and $SM_{40-100\text{ cm}}$ in September in arid areas. The seasonal response of the $\delta^{18}O_{TR}$ to the SM lagged in arid areas. Specifically, the $\delta^{18}O_{TR}$ was significantly negatively correlated with SM at 0–40 cm ($r_{\text{Jun-Aug}} = -0.49$ to -0.41 , $p < 0.05$) in the JA and WA regions, while it was negatively correlated with the SM at all depths ($r_{\text{Jun-Aug}} = -0.44$ to -0.26 , $p < 0.05$) in the WA region. However, the $\delta^{18}O_{TR}$ was significantly negatively correlated at all depths in the MA region ($r_{\text{Jun-Sep}} = -0.47$ to -0.31 , $p < 0.05$), while the $\delta^{18}O_{TR}$ was more significantly negatively correlated with $SM_{40-100\text{ cm}}$ from July to September ($r_{\text{Jun-Sep}} = -0.48$ to -0.29 , $p < 0.05$) in the KA and DE regions.

3.4. The Correlation between $\delta^{18}O_{TR}$ and Key Factors during the Growing Season

The $\delta^{18}O_{TR}$ and the SM showed high correlations during the growing season (June–September). Therefore, the partial correlation analysis was further used to study the most important climatic factors affecting the $\delta^{18}O_{TR}$ (Table 2). The results found that $\delta^{18}O_{TR}$ was significantly negatively correlated with the SM at 0–10 cm in the JA region when VPD and RH were controlled. And the $\delta^{18}O_{TR}$ was significantly correlated with the SM at 0–10 and 10–40 cm in the WA and GA regions. The $\delta^{18}O_{TR}$ was highly significantly negatively correlated with SM at all depths in the MA region when VPD and RH were controlled. However, the $\delta^{18}O_{TR}$ was significantly negatively correlated with the SM at 40–100 cm in the KA and DE regions.

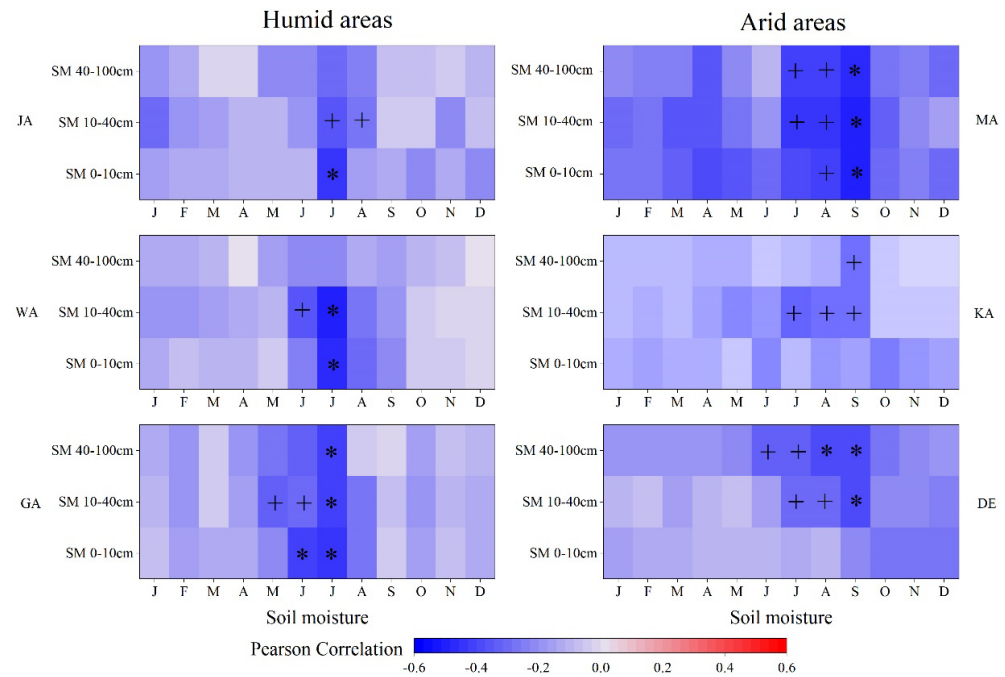


Figure 9. Correlations of $\delta^{18}\text{O}_{\text{TR}}$ with monthly SM. “+”: $p < 0.05$. “*”: $p < 0.01$.

Table 2. Partial correlation analysis between $\delta^{18}\text{O}_{\text{TR}}$ and environmental factors from June–September.

Control Variables	Correlations with $\delta^{18}\text{O}_{\text{TR}}$	JA	WA	GA	MA	KA	DE
VPD	VMC _{0–10}	−0.396 **	−0.364 *	−0.409 *	−0.459 *	−0.211	−0.145
	VMC _{10–40}	−0.265	−0.360 *	−0.383 *	−0.472 *	−0.277	−0.286
	VMC _{40–100}	−0.210	−0.225	−0.241	−0.416 *	−0.356*	−0.385 *
	PDSI	−0.161	−0.106	−0.255	−0.264	−0.278	−0.585 **
PDSI	RH	0.270	0.179	0.423 *	0.151	−0.064	−0.163
	VMC _{0–10}	−0.251	−0.459 *	−0.365 *	−0.527 **	−0.004	0.173
	VMC _{10–40}	−0.213	−0.451 *	−0.317	−0.542 **	−0.118	0.164
	VMC _{40–100}	−0.14	−0.156	−0.343	−0.500 **	−0.239	0.119
RH	VPD	0.057	0.432	−0.141	−0.314	0.003	−0.021
	RH	0.072	−0.396 *	0.251	−0.028	−0.042	−0.022
	VMC _{0–10}	−0.356 **	−0.377 *	−0.392 *	−0.53 **	−0.213	−0.130
	VMC _{10–40}	−0.289	−0.380 *	−0.365 *	−0.542 **	−0.276	−0.274
	VMC _{40–100}	−0.214	−0.225	−0.280	−0.499 *	−0.352 *	−0.365 *
VPD	VPD	0.296	0.259	0.367 *	0.159	−0.042	−0.008
	PDSI	−0.208	−0.113	−0.242	−0.315	−0.277	−0.570 **

“**” indicates $p < 0.05$, and “***” indicates $p < 0.01$.

3.5. The Spatial Patterns of $\delta^{18}\text{O}_{\text{TR}}$ Response to SM with Soil Depths

The response of the $\delta^{18}\text{O}_{\text{TR}}$ to the SM was generally negatively correlated in the study areas (Figure 10). But the correlation of the $\delta^{18}\text{O}_{\text{TR}}$ to the SM at 40–100 cm is stronger than the correlation to the SM at 0–40 cm (Figure 10). And the responses of the $\delta^{18}\text{O}_{\text{TR}}$ to the SM changed from negative to positive as the soil depth deepened in the southern and northeastern parts of the TP (Figure 10). The correlation decreases from the JA region to the DLH region with the SM at 0–10 cm. That means that, as the climate becomes drier, the correlation decreases between the $\delta^{18}\text{O}_{\text{TR}}$ and the SM at 0–40 cm. However, the positive responses of the $\delta^{18}\text{O}_{\text{TR}}$ to the SM at 40–100 cm increase in the DE region.

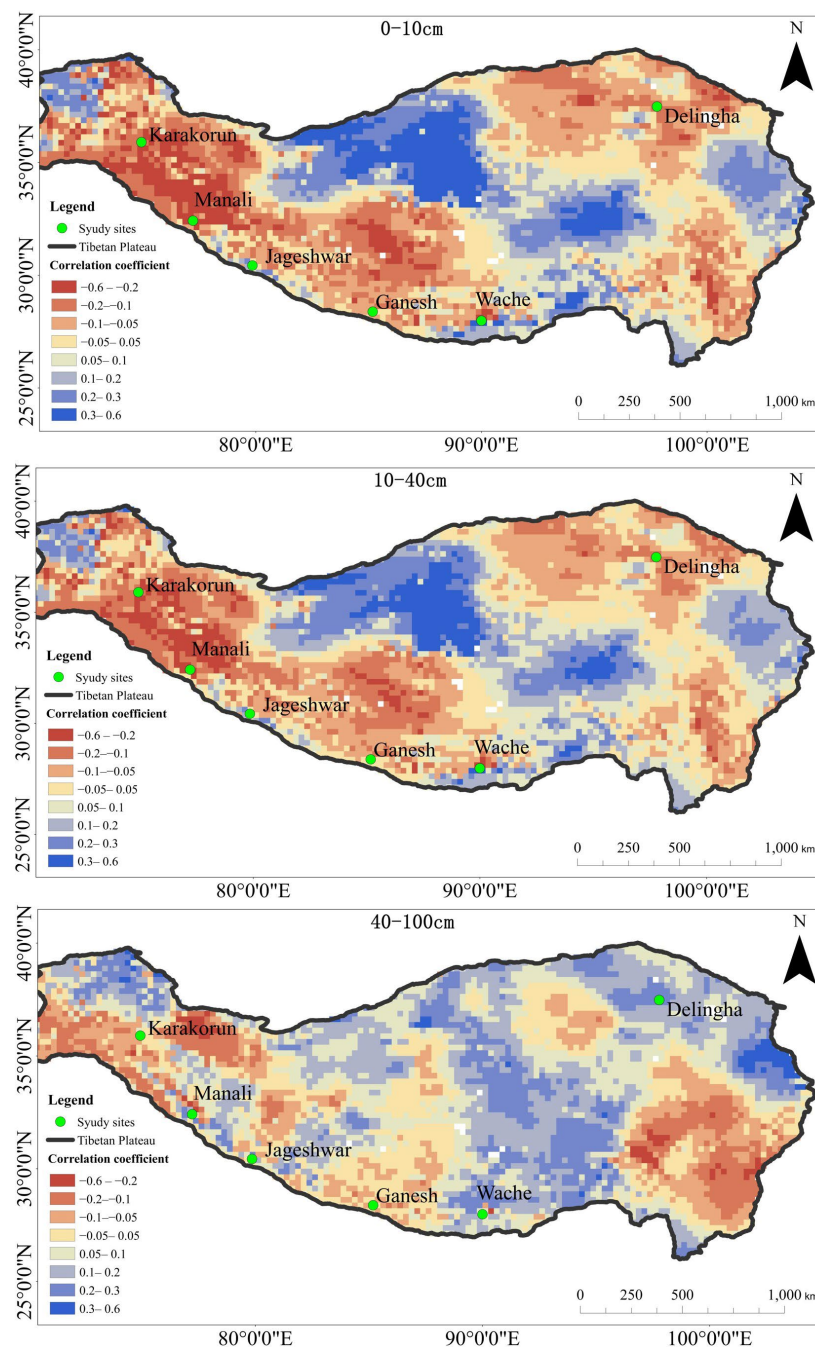


Figure 10. The spatial correlation between SM and $\delta^{18}\text{O}_{\text{TR}}$ in June–September. The green point in the figure represents $\delta^{18}\text{O}_{\text{TR}}$ sampling points. The colors in the graph from red to blue to indicate that the correlation changes from negative to positive.

4. Discussion

4.1. The $\delta^{18}\text{O}_{\text{TR}}$ Records Soil Water Use by Tree Growth on the TP

The temperature has shown a continuous warming trend [41], and precipitation has increased in the eastern and western parts [42,43] and decreased in the southwestern part of the TP since the 1960s [44]. Trees will adopt multiple water use strategies to increase the chances of survival in this context. It has been shown that the $\delta^{18}\text{O}_{\text{TR}}$ could reflect the water uptake of seasons and the depths in trees [19]. This means that the $\delta^{18}\text{O}_{\text{TR}}$ can record soil water $\delta^{18}\text{O}$ information for different seasons and depths [31].

The $\delta^{18}\text{O}_{\text{TR}}$ is mainly controlled by the coupled processes of source water and external climate [15]. In our results, the $\delta^{18}\text{O}_{\text{TR}}$ was more sensitive to the SM than to temperature

during the growing season (Figures 8 and 9). The $\delta^{18}\text{O}_{\text{TR}}$ is derived from the SM, but the $\delta^{18}\text{O}$ of SM varies with soil depths [45]. The isotopic signals in the SM are preserved in the $\delta^{18}\text{O}_{\text{TR}}$ through the xylem during the growing season [46]. Therefore, the $\delta^{18}\text{O}_{\text{TR}}$ can be used as one of the indicators of SM use in trees.

At the same time, the values of the $\delta^{18}\text{O}_{\text{TR}}$ were greater in arid areas (Figure 3). Lower SM leads to an increase in the ratio of internal leaf CO_2 (C_i) to atmospheric CO_2 (C_a) in leaves, which enhances the evaporative enrichment of leaf water in arid areas [47]. Then, the tree root system absorbs heavy-source water, and the $\delta^{18}\text{O}_{\text{TR}}$ is increased further [15]. During the conversion of sucrose produced by tree photosynthesis to cellulose, it undergoes a partial oxygen isotope signal exchange in the source water [48]. In other words, the $\delta^{18}\text{O}_{\text{TR}}$ keeps the mixed signal of source water and leaf evaporation [49]. These two processes result in a higher $\delta^{18}\text{O}_{\text{TR}}$ in arid areas. On the contrary, the decrease in the $\delta^{18}\text{O}_{\text{TR}}$ is due to the reduced evaporation and makes leaf water enrichment weaker in humid areas [50].

4.2. Seasonal Use Strategies of SM for Trees across Wet and Dry Gradients

In climate-sensitive areas, the SM is critical for tree growth. The life history stage [24], season [51], tree species [52], ability of plant access to water [53], and the amount of recent rainfall [14] all have an impact on tree water use strategies. In our study, the $\delta^{18}\text{O}_{\text{TR}}$ was significantly correlated with the SM during the growing season, but the $\delta^{18}\text{O}_{\text{TR}}$ responded to the SM later in arid areas (Figure 9).

The $\delta^{18}\text{O}_{\text{TR}}$ is affected by the SM from June to August in humid areas (Figure 9). Because it is influenced by the ASM and receives adequate precipitation from it in these months, which further affects the $\delta^{18}\text{O}_{\text{TR}}$. These results suggest that monsoon precipitation has a significant effect on tree growth (Figure 8). We believe that precipitation signals in the soil from the ASM are absorbed by tree root systems. Finally, the $\delta^{18}\text{O}$ of precipitation is retained through the $\delta^{18}\text{O}_{\text{TR}}$ in humid areas. Our results have been confirmed in other studies on the TP [31,32].

The $\delta^{18}\text{O}_{\text{TR}}$ are affected by the SM from July to September in arid areas (Figure 9). It is worth noting that the response of the $\delta^{18}\text{O}_{\text{TR}}$ to the SM lagged in arid areas. We believe this is related to the extended growing season of trees on the TP [36]. However, there are significant differences within the arid areas. The $\delta^{18}\text{O}_{\text{TR}}$ in the MA region was controlled by summer monsoon precipitation and RH [54]. And trees mainly absorb winter snowfall in the KA region, which provides a stable water source [37]. Therefore, the correlation between the $\delta^{18}\text{O}_{\text{TR}}$ and the summer SM is not high in the KA region. In the DE region, the $\delta^{18}\text{O}_{\text{TR}}$ was controlled by the SM from May to September [53], and this observation is consistent with that of our study.

The summer precipitation has a greater effect on the SM in the southeastern part of the TP [38]. And the $\delta^{18}\text{O}_{\text{TR}}$ was significantly negatively correlated with precipitation during the growing season in Southern Mexico [55], Northwestern Tibetan Plateau [56], and Ordos Plateau [57]. This is because summer precipitation replenishes plant water supplies [20]. Therefore, the correlation between the SM and precipitation is higher in the southeastern part of the TP than in its northwestern part.

4.3. Depth Use Strategies of SM for Trees across Wet and Dry Gradients

As a typical climate-sensitive area, the TP has a very high spatial variability in precipitation [58]. As a result, trees flexibly adjust their water use strategies to ensure growth. Trees use the deep SM preferentially in arid areas [44], whereas they use the shallow SM in humid areas [59]. This is consistent with our results. However, the water use strategies for trees in complex environments deserve further research.

The $\delta^{18}\text{O}_{\text{TR}}$ was significantly negatively correlated with the SM at 0–10 cm in the JA region. The $\delta^{18}\text{O}_{\text{TR}}$ were significantly negatively correlated with the SM at 0–10 and 10–40 cm after the VPD or RH was controlled in the WA and GA regions (Table 2). This suggests that trees tended to take up the SM in the surface and middle layers in humid

areas. Meanwhile, the surface soil can provide nutrients to the trees [4,60]. In other words, trees preferentially absorb SM on the surface in humid areas.

The significant negative correlation between the $\delta^{18}\text{O}_{\text{TR}}$ and the SM at 40–100 cm in the KA and DE regions was revealed in arid areas (Table 2). In arid areas, capillary water induces trees to form deeper root systems to absorb deep soil water and groundwater to meet higher transpiration needs during the dry season [61,62]. The highly significant negative correlation between the $\delta^{18}\text{O}_{\text{TR}}$ and the SM at all depths in the MA region can be explained by the fact that some SM isotope signals are masked by strong evaporation [63,64]. On the other hand, the “bimodal” precipitation pattern may encourage trees to develop a well-developed root system in this region.

Trees have different coping strategies to climate extremes [60,65]. Trees using a single water strategy will bear a greater risk of death [27,66]. The chances of facing drought stress are increasing on the TP [67]. Trees face greater challenges for survival in humid areas because of the single use of the shallow SM. We argue for the better monitoring of tree growth in the humid regions of this region.

5. Conclusions

In this study, we used the $\delta^{18}\text{O}_{\text{TR}}$ at six sites to investigate whether there are differences in water use strategies of trees across wet and dry gradients on the TP. The results indicated that the SM during the growing season was the main factor influencing tree growth. Trees mainly absorbed the shallow SM in the humid areas, whereas they mainly absorbed the deep SM in the arid areas. And the response of the $\delta^{18}\text{O}_{\text{TR}}$ to the SM in the arid areas lagged behind that in the humid areas. Our study provides a theoretical basis for the further use of $\delta^{18}\text{O}_{\text{TR}}$ to study how tree growth adapts to the SM changes. We argue that shallow soil water uptake is a threat to tree growth in the context of warming on the TP. Therefore, the monitoring of tree growth in the southeastern part of the region should be conducted further.

Author Contributions: Q.L., formal analysis, data curation, visualization, and writing—original draft preparation. L.J., funding acquisition. R.X., writing—original draft. X.C., investigation. P.Z., editing. X.W., supervision. X.Y., investigation. All authors have read and agreed to the published version of the manuscript.

Funding: This research was supported by National Natural Science Foundation of China (No. 42371038), Basic Research Innovation Group Project of Gansu Province (No. 22JR5RA129), and the 2022 Major Scientific Research Project Cultivation Plan of Northwest Normal University (NWNLU-LKZD2022-04). We also thank the anonymous referees for their helpful comments on the manuscript.

Data Availability Statement: The data presented are available on request from the corresponding author of this study.

Conflicts of Interest: The authors declare no conflicts of interest.

References

1. Keyimu, M.; Li, Z.; Liu, G.; Fu, B.; Fan, Z.; Wang, X.; Halik, U. Tree-ring based minimum temperature reconstruction on the southeastern Tibetan Plateau. *Quat. Sci. Rev.* **2021**, *251*, 106712. [[CrossRef](#)]
2. Wang, J.; Taylor, A.R.; D’Orangeville, L. Warming-induced tree growth may help offset increasing disturbance across the Canadian boreal forest. *Proc. Natl. Acad. Sci. USA* **2023**, *120*, e2212780120. [[CrossRef](#)] [[PubMed](#)]
3. Seddon, A.W.; Macias-Fauria, M.; Long, P.R.; Benz, D.; Willis, K.J. Sensitivity of global terrestrial ecosystems to climate variability. *Nature* **2023**, *531*, 229–232. [[CrossRef](#)]
4. Priyadarshini, K.V.R.; Prins, H.H.; Bie, S.; Heitkönig, I.M.; Woodborne, S.; Gort, G.; Kroon, H. Seasonality of hydraulic redistribution by grasses and changes in their water-source use that change tree-grass interactions. *Ecohydrology* **2016**, *9*, 218–228. [[CrossRef](#)]
5. Amer, A.; Franceschi, E.; Hjazin, A. Structure and Ecosystem Services of Three Common Urban Tree Species in an Arid Climate City. *Forests* **2023**, *14*, 671. [[CrossRef](#)]
6. Eslaminejad, P.; Heydari, M.; Kakhki, F.V.; Mirab-balou, M.; Omidipour, R.; Muñoz-Rojas, M.; Lucas-Borja, M.E. Plant species and season influence soil physicochemical properties and microbial function in a semi-arid woodland ecosystem. *Plant Soil* **2020**, *456*, 43–59. [[CrossRef](#)]

7. Ma, J.; Han, J.; Zhang, Y.; Dong, Q.; Lei, N.; Liu, Z.; Du, Y. Temporal stability of soil water content on slope during the rainy season in gully regulation watershed. *Environ. Earth Sci.* **2020**, *79*, 173. [[CrossRef](#)]
8. Bertrand, G.; Masini, J.; Goldscheider, N.; Meeks, J.; Lavastre, V.; Celle-Jeanton, H.; Hunkeler, D. Determination of spatiotemporal variability of tree water uptake using stable isotopes ($\delta^{18}\text{O}$, $\delta^2\text{H}$) in an alluvial system supplied by a high-altitude watershed, Pfyn forest, Switzerland. *Ecohydrology* **2014**, *7*, 319–333. [[CrossRef](#)]
9. Wang, H.; Tetzlaff, D.; Soulsby, C. Modelling the effects of land cover and climate change on soil water partitioning in a boreal headwater catchment. *J. Hydrol.* **2018**, *558*, 520–531. [[CrossRef](#)]
10. Zeng, Q.; Rossi, S.; Yang, B.; Qin, C.; Li, G. Environmental drivers for cambial reactivation of *Qilian junipers* (*Juniperus przewalskii*) in a semi-arid region of northwestern China. *Atmosphere* **2020**, *11*, 232. [[CrossRef](#)]
11. Zhang, F.; Jia, W.; Zhu, G.; Shi, Y.; Zhang, M. Using stable isotopes to investigate differences of plant water sources in subalpine habitats. *Hydrol. Process.* **2022**, *36*, e14518. [[CrossRef](#)]
12. Gao, S.; Liu, R.; Zhou, T.; Fang, W.; Yi, C.; Lu, R.; Luo, H. Dynamic responses of tree-ring growth to multiple dimensions of drought. *Glob. Change Biol.* **2018**, *24*, 5380–5390. [[CrossRef](#)] [[PubMed](#)]
13. Bose, T.; Sengupta, S.; Chakraborty, S.; Borgaonkar, H. Reconstruction of soil water oxygen isotope values from tree ring cellulose and its implications for paleoclimate studies. *Quat. Int.* **2016**, *425*, 387–398. [[CrossRef](#)]
14. Xu, Q.; Li, H.; Chen, J.; Cheng, X.; Liu, S.; An, S. Water use patterns of three species in subalpine forest, Southwest China: The deuterium isotope approach. *Ecohydrology* **2011**, *4*, 236–244. [[CrossRef](#)]
15. Roden, J.S.; Lin, G.; Ehleringer, J.R. A mechanistic model for interpretation of hydrogen and oxygen isotope ratios in tree-ring cellulose. *Geochim. Cosmochim. Acta* **2000**, *64*, 21–35. [[CrossRef](#)]
16. Wright, I.J.; Reich, P.B.; Westoby, M. Least-cost input mixtures of water and nitrogen for photosynthesis. *Am. Nat.* **2003**, *161*, 98–111. [[CrossRef](#)] [[PubMed](#)]
17. Xiao, H.; Deng, W.; Wei, G.; Chen, J.; Zheng, X.; Shi, T.; Zeng, T. A pilot study on zinc isotopic compositions in shallow-water coral skeletons. *Geochem. Geophys. Geosyst.* **2020**, *21*, e2020GC009430. [[CrossRef](#)]
18. Deurwaerder, H.; Hervé-Fernández, P.; Stahl, C.; Burban, B.; Petronelli, P.; Hoffman, B.; Verbeeck, H. Liana and tree below-ground water competition-evidence for water resource partitioning during the dry season. *Tree Physiol.* **2018**, *38*, 1071–1083. [[CrossRef](#)] [[PubMed](#)]
19. Gessler, A.; Ferrio, J.P.; Hommel, R.; Treydte, K.; Werner, R.A.; Monson, R.K. Stable isotopes in tree rings: Towards a mechanistic understanding of isotope fractionation and mixing processes from the leaves to the wood. *Tree Physiol.* **2014**, *34*, 796–818. [[CrossRef](#)]
20. Hahm, W.J.; Dralle, D.N.; Rempe, D.M.; Bryk, A.B.; Thompson, S.E.; Dawson, T.E.; Dietrich, W.E. Low subsurface water storage capacity relative to annual rainfall decouples Mediterranean plant productivity and water use from rainfall variability. *Geophys. Res. Lett.* **2019**, *46*, 6544–6553. [[CrossRef](#)]
21. Lind, M.; Zhang, L.; Falste, D.; Franklin, O.; Brännström, A. Plant diversity and drought: The role of deep roots. *Ecol. Modell.* **2014**, *290*, 85–93. [[CrossRef](#)]
22. Baker, J.C.A.; Gloor, M.; Spracklen, D.V.; Arnold, S.R.; Tindall, J.C.; Clerici, S.J.; Brienen, R.J.W. What drives interannual variation in tree ring oxygen isotopes in the Amazon. *Geophys. Res. Lett.* **2016**, *43*, 11–831. [[CrossRef](#)]
23. Wang, L.; Liu, H.; Leavit, S.; Cresse, E.L.; Quine, T.A.; Shi, J.; Shi, S. Tree-ring $\delta^{18}\text{O}$ identifies similarity in timing but differences in depth of soil water uptake by trees in mesic and arid climates. *Agric. For. Meteorol.* **2021**, *308*, 108569. [[CrossRef](#)]
24. Yang, B.; Wen, X.; Sun, X. Seasonal variations in depth of water uptake for a subtropical coniferous plantation subjected to drought in an East Asian monsoon region. *Agric. For. Meteorol.* **2015**, *201*, 218–228. [[CrossRef](#)]
25. Sun, J.; Ye, C.; Liu, M.; Wang, Y.; Chen, J.; Wang, S.; Tsubo, M. Response of net reduction rate in vegetation carbon uptake to climate change across a unique gradient zone on the Tibetan Plateau. *Environ. Res.* **2022**, *203*, 111894. [[CrossRef](#)] [[PubMed](#)]
26. Wong, J.; Fong, A.; McVicar, N.; Smith, S.; Giambattista, J.; Wells, D.; Alexander, A. Comparing deep learning-based auto-segmentation of organs at risk and clinical target volumes to expert inter-observer variability in radiotherapy planning. *Radiother. Oncol.* **2020**, *144*, 152–158. [[CrossRef](#)] [[PubMed](#)]
27. Fang, O.; Zhang, Q.B. Tree resilience to drought increases in the Tibetan Plateau. *Glob. Change Biol.* **2019**, *25*, 245–253. [[CrossRef](#)]
28. Ge, F.; Sielmann, F.; Zhu, X.; Fraedrich, K.; Zhi, X.; Peng, T.; Wang, L. The link between Tibetan Plateau monsoon and Indian summer precipitation: A linear diagnostic perspective. *Clim. Dyn.* **2017**, *49*, 4201–4215. [[CrossRef](#)]
29. Tan, L.; Cai, Y.; Edwards, L.R.; Lan, J.; Zhang, H.; Gao, Y. High resolution monsoon precipitation changes on southeastern Tibetan Plateau over the past 2300 years. *Quat. Sci. Rev.* **2018**, *195*, 122–132. [[CrossRef](#)]
30. Griebinger, J.; Bräuning, A.; Helle, G.; Schleser, G.H.; Hochreuther, P.; Meier, W.J.H.; Zhu, H. A dual stable isotope approach unravels common climate signals and species-specific responses to environmental change stored in multi-century tree-ring series from the Tibetan plateau. *Geosciences* **2019**, *9*, 151. [[CrossRef](#)]
31. Xu, C.; Zhu, H.; Nakatsuka, T.; Sano, M.; Li, Z.; Shi, F.; Guo, Z. Sampling strategy and climatic implication of tree-ring cellulose oxygen isotopes of *Hippophae tibetana* and *Abies georgei* on the southeastern Tibetan Plateau. *Int. J. Biometeorol.* **2018**, *63*, 679–686. [[CrossRef](#)] [[PubMed](#)]
32. Sano, M.; Dimri, A.P.; Ramesh, R. Moisture source signals preserved in a 242-year tree-ring $\delta^{18}\text{O}$ chronology in the western Himalaya. *Glob. Planet. Change* **2017**, *157*, 73–82. [[CrossRef](#)]
33. Zhang, J.; Gou, X.; Manzanedo, R.D.; Zhang, F.; Pederson, N. Cambial phenology and xylogenesis of *Juniperus przewalskii* over a climatic gradient is influenced by both temperature and drought. *Agric. For. Meteorol.* **2018**, *260*, 165–175. [[CrossRef](#)]

34. Shi, P.J.; Huang, J.G.; Hui, C.; Grissino-Mayer, H.D.; Tardif, J.; Zhai, L.H.; Li, B.L. Capturing spiral radial growth of conifers using the superellipse to model tree-ring geometric shape. *Front. Plant Sci.* **2015**, *6*, 856. [[CrossRef](#)] [[PubMed](#)]
35. Wernicke, J.; Griesinger, J.; Hochreuther, P.; Bräuning, A. Variability of summer humidity during the past 800 years on the eastern Tibetan Plateau inferred from $\delta^{18}\text{O}$ of tree-ring cellulose. *Clim. Past.* **2014**, *10*, 3327–3356.
36. Sano, M.; Tshering, P.; Komori, J. May–September precipitation in the Bhutan Himalaya since 1743 as reconstructed from tree ring cellulose $\delta^{18}\text{O}$. *J. Geophys. Res. Atmos.* **2013**, *118*, 8399–8410. [[CrossRef](#)]
37. Treydte, K.S.; Schleser, G.H.; Helle, G. The twentieth century was the wettest period in northern Pakistan over the past millennium. *Nature* **2006**, *440*, 1179–1182. [[CrossRef](#)] [[PubMed](#)]
38. Yang, B.; Qin, C.; Bräuning, A. Long-term decrease in Asian monsoon rainfall and abrupt climate change events over the past 6,700 years. *Proc. Natl. Acad. Sci. USA* **2021**, *118*, e2102007118. [[CrossRef](#)] [[PubMed](#)]
39. Zeng, X.; Li, X.; Evans, M.N.; Wang, W.; An, W.; Xu, G.; Wu, G. Seasonal incursion of Indian Monsoon humidity and precipitation into the southeastern Qinghai–Tibetan Plateau inferred from tree ring $\delta^{18}\text{O}$ values with intra-seasonal resolution. *Earth Planet. Sci. Lett.* **2016**, *443*, 9–19. [[CrossRef](#)]
40. Murray, F.W. *On the Computation of Saturation Vapor Pressure*; Rand Corporation: Santa Monica, CA, USA, 1966.
41. New, M.; Hulme, M.; Jones, P. Representing twentieth-century space-time climate variability. Part I: Development of a 1961–90 mean monthly terrestrial climatology. *J. Clim.* **1999**, *12*, 829–856. [[CrossRef](#)]
42. Duan, A.; Xiao, Z. Does the climate warming hiatus exist over the Tibetan Plateau? *Sci. Rep.* **2015**, *5*, 13711. [[CrossRef](#)]
43. Jiao, L.; Jiang, Y.; Zhang, W.; Wang, M.; Wang, S.; Liu, X. Assessing the stability of radial growth responses to climate change by two dominant conifer trees species in the Tianshan Mountains, northwest China. *For. Ecol. Manag.* **2019**, *433*, 667–677. [[CrossRef](#)]
44. Li, Y.; Peng, S.; Liu, H.; Zhang, X.; Ye, W.; Han, Q.; Li, Y. Westerly jet stream controlled climate change mode since the Last Glacial Maximum in the northern Qinghai–Tibet Plateau. *Earth Planet. Sci. Lett.* **2020**, *549*, 116529. [[CrossRef](#)]
45. Hu, S.; Zhou, T.; Wu, B. Impact of developing ENSO on Tibetan Plateau summer rainfall. *J. Clim.* **2021**, *34*, 3385–3400. [[CrossRef](#)]
46. Li, Q.; Liu, Y.; Nakatsuka, T.; Fang, K.; Song, H.; Liu, R.; Wang, K. East Asian Summer Monsoon moisture sustains summer relative humidity in the southwestern Gobi Desert, China: Evidence from $\delta^{18}\text{O}$ of tree rings. *Clim. Dyn.* **2019**, *52*, 6321–6337. [[CrossRef](#)]
47. Farquhar, G.D.; Lloyd, J. Carbon and oxygen isotope effects in the exchange of carbon dioxide between terrestrial plants and the atmosphere. In *Stable Isotopes and Plant Carbon–Water Relations*; Academic Press: Cambridge, MA, USA, 1993; pp. 47–70.
48. Mirfenderesgi, G.; Bohrer, G.; Matheny, A.M.; Fatichi, S.; Schäfer, K.V. Tree level hydrodynamic approach for resolving above-ground water storage and stomatal conductance and modeling the effects of tree hydraulic strategy. *J. Geophys. Res. Biogeosci.* **2016**, *121*, 1792–1813. [[CrossRef](#)]
49. Zhan, N.; Wang, Z.; Xie, Y.; Shang, X.; Liu, G.; Wu, Z. Expression patterns and regulation of non-coding RNAs during synthesis of cellulose in *Eucalyptus grandis* Hill. *Forests* **2021**, *12*, 1565. [[CrossRef](#)]
50. Giraldo, J.A.; Valle, J.I.; González-Caro, S.; Sierra, C.A. Intra-annual isotope variations in tree rings reveal growth rhythms within the least rainy season of an ever-wet tropical forest. *Trees* **2022**, *36*, 1039–1052. [[CrossRef](#)]
51. Rao, W.; Chen, X.; Meredith, K.T.; Tan, H.; Gao, M.; Liu, J. Water uptake of riparian plants in the lower Lhasa River Basin, South Tibetan Plateau using stable water isotopes. *Hydrol. Process.* **2020**, *34*, 3492–3505. [[CrossRef](#)]
52. Van, T.; Verheyen, K.; Kint, V.; Van, E.; Muys, B. Plasticity of tree architecture through interspecific and intraspecific competition in a young experimental plantation. *For. Ecol. Manag.* **2017**, *385*, 1–9.
53. Schwendenmann, L.; Pendall, E.; Sanchez-Bragado, R.; Kunert, N.; Hölscher, D. Tree water uptake in a tropical plantation varying in tree diversity: Interspecific differences, seasonal shifts and complementarity. *Ecohydrology* **2015**, *8*, 1–12. [[CrossRef](#)]
54. Zhang, J.; Gou, X.; Alexander, M.R.; Xia, J.; Wang, F.; Zhang, F.; Pederson, N. Drought limits wood production of *Juniperus przewalskii* even as growing seasons lengthens in a cold and arid environment. *Catena* **2021**, *196*, 104936. [[CrossRef](#)]
55. Brienen, R.J.; Hietz, P.; Wanek, W.; Gloor, M. Oxygen isotopes in tree rings record variation in precipitation $\delta^{18}\text{O}$ and amount effects in the south of Mexico. *J. Geophys. Res. Biogeosci.* **2013**, *118*, 1604–1615. [[CrossRef](#)]
56. Guo, X.; Tian, L. Spatial patterns and possible mechanisms of precipitation changes in recent decades over and around the Tibetan Plateau in the context of intense warming and weakening winds. *Clim. Dyn.* **2022**, *59*, 2081–2102. [[CrossRef](#)]
57. Liu, Y.; Wang, L.; Li, Q. Asian summer monsoon-related relative humidity recorded by tree ring $\delta^{18}\text{O}$ during last 205 years. *J. Geophys. Res. Atmos.* **2019**, *124*, 9824–9838. [[CrossRef](#)]
58. Li, F.F.; Lu, H.L.; Wang, G.Q.; Yao, Z.Y.; Li, Q.; Qiu, J. Zoning of precipitation regimes on the Qinghai–Tibet Plateau and its surrounding areas responded by the vegetation distribution. *Sci. Total Environ.* **2022**, *838*, 155844. [[CrossRef](#)]
59. Holdo, R.M.; Nippert, J.B.; Mack, M.C. Rooting depth varies differentially in trees and grasses as a function of mean annual rainfall in an African savanna. *Oecologia* **2018**, *186*, 269–280. [[CrossRef](#)]
60. Zhou, Y.; Chen, S.; Song, W.; Lu, Q.; Lin, G. Water-use strategies of two desert plants along a precipitation gradient in northwestern China. *J. Plant Ecol.* **2011**, *35*, 789. [[CrossRef](#)]
61. Sun, L.; Yang, L.; Chen, L.; Zhao, F.; Li, S. Short-term changing patterns of stem water isotopes in shallow soils underlain by fractured bedrock. *Hydrol. Res.* **2019**, *50*, 577–588. [[CrossRef](#)]
62. Grossiord, C.; Sevanto, S.; Dawson, T.E.; Adams, H.D.; Collins, A.D.; Dickman, L.T.; McDowell, N.G. Warming combined with more extreme precipitation regimes modifies the water sources used by trees. *New Phytol.* **2017**, *213*, 584–596. [[CrossRef](#)]
63. Oerter, E.; Finstad, K.; Schaefer, J.; Goldsmith, G.R.; Dawson, T.; Amundson, R. Oxygen isotope fractionation effects in soil water via interaction with cations (Mg, Ca, K, Na) adsorbed to phyllosilicate clay minerals. *J. Hydrol.* **2014**, *515*, 1–9. [[CrossRef](#)]

64. Dai, Y.; Zheng, X.J.; Tang, L.S.; Li, Y. Stable oxygen isotopes reveal distinct water use patterns of two *Haloxylon* species in the Gurbantonggut Desert. *Plant Soil* **2015**, *389*, 73–87. [[CrossRef](#)]
65. Tron, S.; Bodner, G.; Laio, F. Can diversity in root architecture explain plant water use efficiency? A modeling study. *Ecol. Modell.* **2015**, *312*, 200–210. [[CrossRef](#)] [[PubMed](#)]
66. Xue, R.; Jiao, L.; Zhang, P.; Du, D.; Wu, X.; Wei, M.; Li, Q.; Wang, X.; Qi, C. The key role of ecological resilience in radial growth processes of conifers under drought stress in the subalpine zone of marginal deserts. *Sci. Total Environ.* **2023**, *903*, 166864. [[CrossRef](#)]
67. Yao, Y.; Liu, Y.; Zhou, S.; Son, J.; Fu, B. Soil moisture determines the recovery time of ecosystems from drought. *Glob. Change Biol.* **2013**, *29*, 3562–3574. [[CrossRef](#)]

Disclaimer/Publisher’s Note: The statements, opinions and data contained in all publications are solely those of the individual author(s) and contributor(s) and not of MDPI and/or the editor(s). MDPI and/or the editor(s) disclaim responsibility for any injury to people or property resulting from any ideas, methods, instructions or products referred to in the content.